APPLICATION OF THE BALANCED HYBRID MODE IN OVERMODED CORRUGATED WAVEGUIDES TO SHORT WAVELENGTH DYNAMIC UNDULATORS

M. Shumail[#], G. B. Bowden, C. Chang, J. Neilson, S. G. Tantawi, SLAC, Menlo Park, CA 94025
C. Pellegrini, UCLA, CA 90095, U.S.A.

Abstract

Inspired by recent developments in low-loss overmoded components and systems for ultra-high power RF systems, we explored several overmoded waveguide systems that could function as RF undulators. One promising structure is a corrugated waveguide system operating at the balanced hybrid HE_{11} mode. This is a new application for that mode. Initial calculations indicate that such a system can be operated at relatively low power levels (~ 50 MW) while obtaining large values for the undulator parameters $K \sim 1$. RF surface fields are typically low enough to permit superconducting operation. This technology can realize an undulator with short wavelengths and gives dynamic control of the undulator parameters including polarization. We introduce the scaling laws governing such structures, and establish the superiority of the balanced hybrid HE_{11} mode by comparative analysis. The scaling laws are verified through exact simulations. High quality factor of HE_{11} mode is demonstrated through measurements of a prototype design. Finally, a novel design is presented with low surface fields.

INTRODUCTION

The dynamic RF undulators promise to impart a convenient control over the polarization and wavelength of the FEL radiation. Moreover, the large transverse radius of the overmoded waveguide weakens the effect of the wakefields [1-5].

In our analysis, we assume an undulator to be in the form of a circular cylindrical RF cavity, with either a smooth conducting wall or a finite constant impedance wall, of length L and radius a. The device lies symmetrically about the z-axis along which we expect the electron beam to travel.

Following notation is used for various RF parameters: frequency (f), angular frequency ($\omega = 2\pi f$), free space RF wavelength (λ), propagation constant along z-axis (β), and free space wavenumber $k = \frac{2\pi}{\lambda}$. The normalized length is defined as $\tilde{L} = \frac{L}{\lambda}$. However, to facilitate the comparison among various modes, we define the normalized radius as $\tilde{a} = \frac{a}{a_c} \geq 1$, where a_c is, exactly (for TE_{1n}) or approximately (for HE_{1n}), the mode cutoff radius. In terms of the normalized radius, the propagation constant can be expressed as:

$$\beta = \frac{2\pi}{\lambda}\sqrt{1 - \tilde{a}^{-2}} \qquad (1)$$

The modes of interest for any on-axis RF undulator,

with cylindrical symmetry, are TM_{1n}, TE_{1n}, and HE_{1n} modes. For any given set of parameters, TE_{1n} modes turn out to be superior to TM_{1n} modes. In this paper, we present the scaling laws for the linearly polarized TE_{1n} and HE_{1n} modes. A comparison of these modes demonstrates the promising features of the HE_{11} mode.

We also present the cold test results of a prototype corrugated cavity, and show that a high quality factor (Q_0) can be achieved for a HE_{11} mode. In the end, we present our recent design of an RF undulator that exhibits low surface fields on the end walls.

ZERO-IMPEDANCE-ADMITTANCE SURFACE FOR BALANCED HYBRID MODES

For balanced hybrid modes, the impedance and admittance of the constant impedance wall should be vanishingly small [6-7]. In this case, the transverse field components of HE_{1n} modes become proportional to $J_0(s)$, the Bessel function of order 0. This gives a unique feature to the balanced hybrid HE_{1n} modes that all its transverse fields are more concentrated on the axis and tend to vanish near the surface.

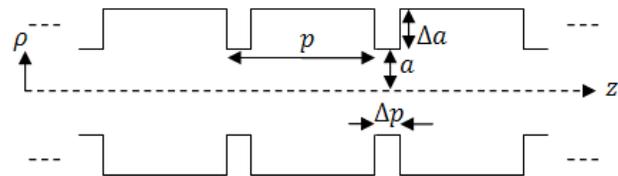Such a surface can be implemented by transverse corrugations of a metallic cylindrical wall, as shown in Fig. 1.

Figure 1: Longitudinal cross-section of a constant impedance cylindrical surface.

In Fig. 1, the corrugation period p is less than $\lambda/2$, hence the slots can only support TM fields with field components, E_z, B_φ, and B_ρ. Thus, at $\rho = a^-$, $E_\varphi = 0$, while there is a finite magnetic field B_z. Thus the normalized surface impedance $\tilde{Z} = -i\left(\frac{E_\varphi}{c\,B_z}\right)_{\rho \to a^-}$ vanishes. Moreover, it can be shown, that for $ka \gg 1$, the normalized surface admittance $\tilde{Y} = i\left(\frac{c\,B_\varphi}{E_z}\right)_{\rho \to a^-}$ almost equals $-\cot k\Delta a$ [6] and hence vanishes for slot depth $\Delta a \approx \frac{\lambda}{4}$. In this way a so called zero-impedance-admittance surface is obtained. In practice, the value of $p < \lambda/2$ is selected to yield resonant condition for the

[#]shumail@slac.stanford.edu

02 Synchrotron Light Sources and FELs

T15 Undulators and Wigglers

desired frequency. The value of Δa can then be tuned around $\frac{\lambda}{4}$ for optimal results, like lower power loss and surface fields. The slot thickness Δp needs to be just large enough to maintain the minimum aspect ratio for mechanical considerations. Generally, $\Delta p = \frac{\lambda}{16}$ is a good choice.

SCALING LAWS

In the context of insertion devices, it seems appropriate to define following scaling factors for fields, energy, and power in terms of the undulator parameter K, normalized RF wavelength $\tilde{\lambda} = \lambda/1$ cm, and normalized conductivity $\tilde{\sigma}$ (= 1 for copper).

$$E_0 = 4\pi \, \frac{m\,c}{e} \, \frac{c}{\lambda} \, K = 642 \text{ MV m}^{-1} \, \tilde{\lambda}^{-1} \, K \tag{2}$$

$$B_0 = -i \, E_0/c = -i \, 2140 \text{ mT } \tilde{\lambda}^{-1} \, K \tag{3}$$

$$U_0 = \frac{2\pi}{\mu_0} \left(\frac{m\,c}{e} \right)^2 K^2 = 14.5 \text{ Joules m}^{-1} \, K^2 \tag{4}$$

$$P_0 = 8\pi \left(\frac{m\,c}{\mu_0\,e} \right)^2 \sqrt{\left(\frac{\pi f \, \mu_0}{\tilde{\sigma} \, (5.8 \, 10^7 \, S \, m^{-1})} \right)} K^2$$
$$= 2.089 \text{ MW } \tilde{\sigma}^{-1/2} \, \tilde{\lambda}^{-1/2} \, K^2 \tag{5}$$

Here m and e are, respectively, electron mass and charge, c is the speed of light in vacuum, and μ_0 is the free space permeability.

Balanced Hybrid HE_{1n} modes

Observing the fact that $u_{1n} \approx s_{0n}$(zeros of $J_0(s)$) for a Hybrid balanced HE_{1n} mode, we define normalized radial coordinate s and normalized radius $\tilde{a}$ as $s = \frac{\rho}{a} s_{0n}$ and $\tilde{a} = \frac{2\pi}{s_{0n}} \frac{a}{\lambda}$. For $\tilde{a} \geq 2$, we can write following approximate expressions for a hybrid balanced HE_{1n} mode:

Propagation constant: $\beta \approx \frac{2\pi}{\lambda} \left(1 - \frac{1}{2} \tilde{a}^{-2} \right)$ (6)

Undulator wavelength: $\lambda_u \approx \frac{\lambda}{2}$ (7)

Cutoff radius: $a_c \approx \frac{s_{0n}}{2\pi} \lambda$ (8)

Field components (phasor form with implicit $e^{i\omega t}$):
$$E_z \approx E_0 \, \tilde{a}^{-1} J_1(s) \, \cos\varphi \, \cos\beta z \tag{9}$$
$$B_z \approx B_0 \, \tilde{a}^{-1} J_1(s) \, \sin\varphi \, \sin\beta z \tag{10}$$
$$E_\rho \approx -E_0 \left(1 - \frac{1}{4}\tilde{a}^{-2} \right) J_0(s) \, \cos\varphi \, \sin\beta z \tag{11}$$
$$E_\varphi \approx E_0 \left(1 - \frac{1}{4}\tilde{a}^{-2} \right) J_0(s) \, \sin\varphi \, \sin\beta z \tag{12}$$
$$B_\rho \approx B_0 \left(1 - \frac{1}{4}\tilde{a}^{-2} \right) J_0(s) \, \sin\varphi \, \cos\beta z \tag{13}$$
$$B_\varphi \approx B_0 \left(1 - \frac{1}{4}\tilde{a}^{-2} \right) J_0(s) \, \cos\varphi \, \cos\beta z \tag{14}$$

Stored energy per unit length:
$$U \approx U_0 \frac{J_1^2(s_{0n})s_{0n}^2}{2} \left(\tilde{a} + \frac{\zeta_1}{s_{0n}} \right)^2$$
$$\approx U_0 \tilde{a}^2 \, (n - 0.25) \tag{15}$$

End wall losses:
$$P_{loss_{end}} \approx P_0 \frac{J_1^2(s_{0n})s_{0n}^2}{2} \left(\tilde{a}^2 - \frac{1}{2} \right)$$
$$\approx P_0 \, (n - 0.25) \left(\tilde{a}^2 - \frac{1}{2} \right) \tag{16}$$

Cylindrical wall losses:
$$P_{loss_{cyl}} \approx \zeta_2 \, P_0 \, \tilde{L} \, \tilde{a}^{-1} J_1^2(s_{0n}) s_{0n} \pi \approx 2 P_0 \, \tilde{L} \, \tilde{a}^{-1} \tag{17}$$

Peak surface fields:
$$E_{peak\_surf} \approx E_0 \, \tilde{a}^{-1} J_1(s_{0n}) \tag{18}$$

$$B_{peak\_surf} \approx B_0 \tag{19}$$

In Eq. (15) and (17), $\zeta_1 \sim 1$ and $\zeta_2 \sim 1$ are adjustment constants, and their values depend on the particular implementation of the zero-impedance-admittance cylindrical wall of the cavity.

TE_{1n} modes

For the sake of comparison, we present here the corresponding expressions for the stored energy per unit length and the losses for TE_{1n} modes. Here, the normalized radius $\tilde{a}$ is defined with respect to the cutoff radius of the corresponding TE_{1n} mode.

$$U = U_0 \, \tilde{a}^2 J_1^2(s'_{1n}) \left(s'^2_{1n} - 1 \right)$$
$$\approx U_0 \, \tilde{a}^2 \, (2n - 0.68) \tag{20}$$
$$P_{loss_{end}} = P_0 \, (\tilde{a}^2 - 1) J_1^2(s'_{1n}) \left(s'^2_{1n} - 1 \right)$$
$$\approx P_0 \, (\tilde{a}^2 - 1) \, (2n - 0.68) \tag{21}$$
$$P_{loss_{cyl}} = P_0 \, \tilde{L} \, \tilde{a} \, J_1^2(s'_{1n}) s'_{1n} \pi$$
$$\left(s'^{-2}_{1n} + \tilde{a}^{-2} \left(1 - s'^{-2}_{1n} \right) \right)$$
$$\approx 2 \, P_0 \, \tilde{L} \, \tilde{a} \left(s'^{-2}_{1n} + \tilde{a}^{-2} \left(1 - s'^{-2}_{1n} \right) \right) \tag{22}$$

Balanced Hybrid HE_{1n} versus TE_{1n} modes

Comparing Eq. $(15 - 17)$ with Eq. $(20 - 22)$, one can guess that the HE_{1n} modes do better than the corresponding TE_{1n} modes. Fig. 2 presents a comparison of TE_{1n} and HE_{1n} modes, in terms of the stored energy (U) and the total losses ($P_{loss} = P_{loss_{end}} + P_{loss_{cyl}}$).
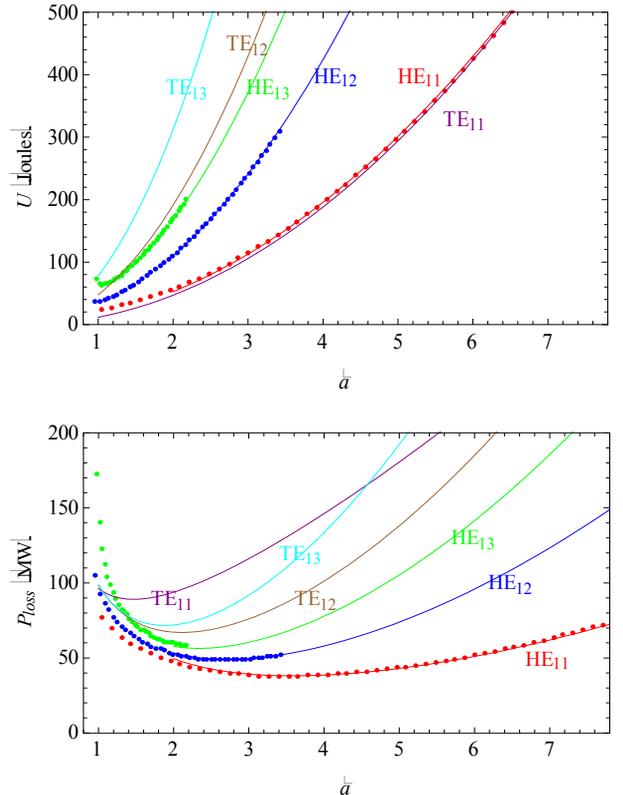

Figure 2: Stored energy (U) and total losses (P_{loss}) versus normalized radius ($\tilde{a}$).

Here, the TE_{1n} modes correspond to a smooth wall cavity, while the HE_{1n} modes correspond to the cavity whose cylindrical surface is a constant impedance wall determined by the parameters: $\Delta a = \frac{\lambda}{4}\left(1 + \frac{1}{k\,a}\right)$, $\Delta p = \frac{\lambda}{16}$, and $p = \frac{2\pi}{3\beta_{HE11}}$. The modes are compared against the same values of their respective normalized radii. We have chosen: $K = \tilde{\sigma} = 1$, $f = 11.424$ GHz, and $L = 1$m. The dots correspond to the exact solution based on mode matching technique [8], while the solid lines are the plots of corresponding analytical expressions, Eq. $(15-17)$ and Eq. $(20-22)$. We choose $\zeta_1 = 0.38$ and $\zeta_2 = 0.92$ to fit the HE_{11} data.

It is obvious that the stored energy and the total power loss associated with the HE_{1n} modes are generally lower, at least for this particular implementation, than that of the corresponding TE_{1n} modes. In particular, HE_{11} mode outperforms all the rest, especially due to the lower associated power loss.

PROTOTYPE TEST

To validate our theoretical findings, we fabricated a prototype corrugated wall cylindrical cavity and measured the quality factors (Q_0) of various modes. The design parameters of this cavity are as follows: $\Delta a = 0.280$ in, $\Delta p = 0.065$ in, $p = 0.416$ in, $a = 2.066$ in, $L = 24p = 9.984$ in, and $\tilde{\sigma} = 0.431$ (Aluminium).

Table 1: Quality Factor for various Modes

Mode	Measured	Calculated
HE_{13} (11.279 GHz)	39,390	46,000
HE_{14} (11.308 GHz)	24,950	27,600
HE_{11} (11.428 GHz)	105,900	120,000
HE_{14} (11.507 GHz)	25,820	29,100
HE_{12} (11693 GHz)	67,100	85,600

Measurements confirm the high quality factor exhibited by the HE_{11} mode. However, all the measured values of Q_0 are about 10% less than the calculated values. The difference is probably due to the lower value of conductivity of the cavity alloy than that of the pure aluminum which is assumed for the calculated results.

UNDULATOR DESIGN WITH LOW SURFACE FIELDS

According to Eq. (3) and (19), the magnetic field on the end walls of the undulator can be as high as 815 mT for $K = 1$, and $\lambda = 2.6242$ cm.

To solve the problem of high peak fields on the end walls near the axis, we introduce a concave design for the end walls which is perpendicular to the local Poynting vectors. Fig. 3 shows such a design along with the plots of the magnitude of electric (E) and magnetic (H) fields along the axis of such an undulator. Such a design can help reduce the peak surface field by a factor of half or so.
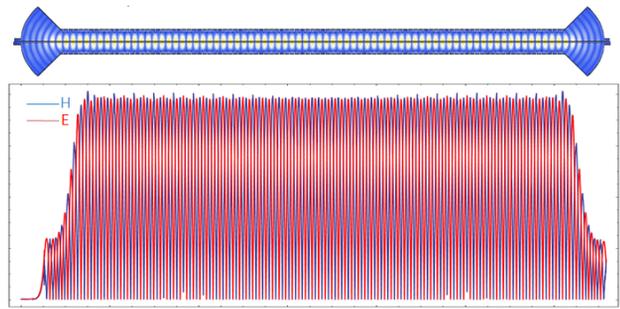

Figure 3: An optimized design of RF undulator and fields along its axis.

CONCLUSION

After a brief discussion about the design strategy of a zero-impedance-admittance wall to support the balanced hybrid HE_{1n} modes, we presented scaling laws for these modes and compared them against the TE_{1n} modes. It turns out that the HE_{1n} modes have generally lower stored energy and exhibit less power loss than the corresponding TE_{1n} modes. Especially, the HE_{11} mode seems to be the most promising one. We also presented results of a prototype design that exhibited high quality factor for the HE_{11} mode. Lastly, we presented a practical undulator design with low peak surface fields on the end walls.

REFERENCES

[1] Tantawi, V. Dolgashev, C. Nantista, C. Pellegrini, J. Rosenzweig, G. Travish, "A coherent compton backscattering high hain FEL using an X-band microwave undulator", FEL Conference 2005, Stanford, California, USA, 2005.

[2] T. Shintake, K. Huke, J. Tanaka, I. Sato and I. Kumabe, "Development of microwave undulator", Japanese J. of Appl. Phys., 22, p. 844-851, 1983.

[3] T.M. Tran, B.G. Danly, J. S. Wurtele, "Free-electron lasers with electromagnetic standing wave wigglers", IEEE J. of Quantum Electronics, Vol. QE-23, pp. 1578-1589, 1987.

[4] M.Yeddulla, H. Geng, Z. Ma, Z. Huang, S. Tantawi, "Waveguide structures for RF undulators with applications to FEL and storage rings", Proceedings of EPAC08, Genoa, Italy, 2008.

[5] S. C. Pellegrini, "X-band microwave undulators for short wavelength free-electron lasers", FEL Conference 2005, Stanford, California, USA, 2005.

[6] P. J. B. Clarricoats, A. D. Olver, "Corrugated horns for microwave antennas", Peter Peregrinus Ltd, London, UK, 1984.

[7] S.F. Mahmoud, "Electromagnetic Waveguides theory and applications", Peter Peregrinus Ltd, London, UK, 1991.

[8] J. Neilson, P. Latham, M. Caplan, W. Lawson, "Determination of the resonant frequencies in a complex cavity using the scattering matrix formulation", IEEE Trans. Microwave Theory and Tech., vol. 37, No. 8, 1989.

02 Synchrotron Light Sources and FELs

T15 Undulators and Wigglers